Effect of suppression of the inelastic scattering rate on the penetration depth and conductivity in a $d_{x^2-y^2}$ superconductor

E. Schachinger and J. P. Carbotte
Department of Physics and Astronomy, McMaster University, Hamilton, Ontario, Canada L8S 4M1

F. Marsiglio
Neutron & Condensed Matter Science, AECL, Chalk River Laboratories, Chalk River, Ontario, Canada K0J 1J0
(Received 22 January 1997)

We use a separable d-wave model to describe the momentum dependence of the pairing interaction in the gap channel. We include the inelastic scattering through a spectral density which describes the fluctuation spectrum responsible for superconductivity. The collapse of the scattering rate observed in microwave experiments is modeled through a low-frequency cutoff on the fluctuation spectrum. The effect of this cutoff on the temperature dependence of the magnetic-field penetration depth and on the infrared conductivity and associated scattering rates is calculated. [S0163-1829(97)06129-8]

I. INTRODUCTION

The magnetic penetration depth in $YBa_2Cu_3O_{7-x}$ (YBCO) is observed to be linear at low temperatures.[1,2] This behavior is consistent with many other experimental data which indicate that the gap has $d_{x^2-y^2}$ symmetry with nodes crossing the Fermi surface.[1–13] While many of the experiments are sensitive only to the magnitude of the gap,[1–8] others have been devised specifically to probe its phase.[9–13] The modifications in the low-temperature linear dependence of the magnetic penetration depth brought about through impurity scattering[2,14] are also naturally understood in a model with an order parameter having d-wave symmetry.[15–17] Such models, however, tend to predict slopes[15–18] for the penetration depth near the critical temperature (T_c) which are not as steep as is observed.[1,2] This is true even when inelastic scattering is incorporated into the calculations through an Eliashberg-type formalism[18] which represents a first approximate attempt at including self-energy effects.[19] This deficiency, common to all simple d-wave models, can be circumvented phenomenologically by noting that the value of the slope of the penetration depth at low temperatures is inversely dependent on the ratio of the maximum gap (Δ/k_BT_c) in the Brillouin zone to the value of T_c. In BCS theory, this ratio is equal to 2.2 but the data over the entire range of temperature, including the region near T_c, can be fit quite well simply by choosing a larger value of Δ/k_BT_c,[20,21] taken to be a fitting parameter. Physically, such a large value of Δ/k_BT_c in the range of 3–4 can be thought of as due to some additional mechanism which limits T_c but not Δ and which is not included in a BCS theory or its simple extensions. One possibility is that thermal fluctuations which reduce T_c below its mean-field value might provide such a mechanism. The penetration depth data have, in fact, been interpreted in this way.[22]

In this paper, we propose a very different explanation. Although, at present, no consensus exists as to the exact nature of the mechanism responsible for the superconductivity in the oxides, most mechanisms proposed so far, which also lead to a d-wave state, are electronic[23–27] in origin (not phonons). As is now well known and widely accepted, an electronic mechanism offers a natural and straightforward explanation for the large low-temperature peak observed[14,28–30] in the microwave conductivity of YBCO. An interpretation of this striking fact, referred to as the collapse of the low-temperature inelastic scattering rates in the superconducting state, is that a gap develops in the fluctuation spectrum which is responsible for the superconductivity.[31,32] Thus, the quasiparticles become very long lived[28,33,34] at low temperature. This effect is generic to all electronic mechanisms in which the fluctuation spectrum which causes the superconductivity belongs to the superconducting electron system itself and becomes gapped as superconductivity sets in.

We begin by recalling that in conventional anisotropic s-wave superconductors the introduction of ordinary elastic impurity scattering is known to reduce the anisotropy and, consequently, the value of T_c. Also, functional derivative methods show that very-low-frequency phonons have the same effect as static impurities and therefore reduce T_c;[35] i.e., they are pair breaking. Similar considerations apply to a d-wave superconductor stabilized by antiferromagnetic spin fluctuations,[36] in which case it has been shown that the functional derivative of T_c with a boson (spin fluctuation) spectral density is negative at low frequencies. This means that at low frequencies boson exchange reduces rather than enhances T_c. If, at low temperatures, such low-energy excitations are removed because of the gapping of the fluctuation spectrum in the superconducting state, we would expect that the superconducting gap itself will be larger than it would otherwise be for the associated value of T_c. Alternatively, as the temperature is increased, the amount of pair breaking increases because the low-frequency part of the boson spectral density is restored as the superconducting gap closes up. This should affect the temperature dependence of the penetration depth and act to move it away from a BCS variation and more towards the experimentally observed variation with a smaller than expected (on a BCS model) slope at low T and a steeper one near T_c.

Besides studying the effect of the gapping of the fluctuation spectrum on the penetration depth, we also study its effect on both the real and imaginary parts of the infrared conductivity and on the associated frequency-dependent scattering rate which can be obtained directly from the conductivity if a generalized Drude form is used. Comparison with experimental data is made and the effects of more general readjustments to the fluctuation spectrum with reduced temperature are also considered.

In Sec. II we give the necessary formalism for the penetration depth including the gap equations. Results are presented and discussed in Sec. III. In Sec. IV the formula for the conductivity is given and results can be found in Sec. V. A short conclusion is given in Sec. VI.

II. FORMALISM

The simplest description of a d-wave superconductor is obtained within a BCS formalism assuming a separable model for the pairing interaction. In such a model, the pairing potential depends on the product $\cos(2\theta)\cos(2\theta')$ where θ and θ' are the directions of the initial and final momenta on a two-dimensional (2D) circular Fermi surface. To include the dynamics of the fluctuations that are exchanged in the pairing, it is necessary to go beyond BCS and consider self-energy corrections in an Eliashberg formalism with a boson-exchange spectral density $I^2F(\Omega)$. This spectral density enters both the gap channel for the pairing energy $\tilde{\Delta}(i\omega_n)$ and the renormalization channel for the renormalized Matsubara frequency $\tilde{\omega}(i\omega_n)$. This last quantity exists in the normal state and carries the information on the direct renormalization due to the interactions in that case. From symmetry considerations, the gap channel involves the d-wave part of the interaction while the renormalization channel involves its s-wave part. In principle, these two projections of the complete boson-exchange interaction need not involve the same weighting of the boson energies. For simplicity here, however, we will assume that a single $I^2F(\Omega)$ can nevertheless be employed as a first approximation but with a different numerical weight g in the $\tilde{\Delta}(i\omega_n)$ channel as compared with the $\tilde{\omega}(i\omega_n)$ channel. The two nonlinear self-energy equations written for $\tilde{\Delta}(i\omega_n)$ and $\tilde{\omega}(i\omega_n)$, respectively, with $i\omega_n=i(2n+1)T$, $n=0,\pm1,\pm2\ldots$, and temperature T have the form[18,19,37]

$$\tilde{\Delta}(i\omega_n;\theta)=\pi T\, g\sum_m \cos(2\theta)\lambda(m-n)\times\left\langle \frac{\cos(2\theta')\tilde{\Delta}(i\omega_m;\theta')}{\sqrt{\tilde{\omega}(i\omega_m)^2+\tilde{\Delta}(i\omega_m;\theta')^2}}\right\rangle' \quad (1)$$

and

$$\tilde{\omega}(i\omega_n)=\omega_n+\pi T\sum_m \lambda(m-n)\times\left\langle \frac{\tilde{\omega}(i\omega_m)}{\sqrt{\tilde{\omega}(i\omega_m)^2+\tilde{\Delta}(i\omega_m;\theta')^2}}\right\rangle', \quad (2)$$

where the brackets $\langle\cdots\rangle'$ indicate an average over the angle θ' of the final electronic states. In Eqs. (1) and (2) the boson spectral density $I^2F(\Omega)$ enters through

$$\lambda(m-n)=2\int_0^\infty d\Omega\,\frac{\Omega I^2F(\Omega)}{\Omega^2+(\omega_m-\omega_n)^2}. \quad (3)$$

We emphasize again that unless one had microscopic information on the precise mechanism causing the superconductivity, a knowledge we do not yet have, introducing a different form for $I^2F(\Omega)$ vs Ω in the two equations (1) and (2) would simply increase the number of arbitrary parameters introduced.

The London penetration depth $\lambda_L(T)$ at any temperature $T<T_c$ follows from the solutions of Eqs. (1) and (2). It is given, within a numerical constant, by[15–19]

$$\frac{1}{\lambda_L^2(T)}\propto\left\langle \pi T\sum_m \frac{\tilde{\Delta}(i\omega_m;\theta)^2}{[\tilde{\omega}(i\omega_m)^2+\tilde{\Delta}(i\omega_m;\theta)^2]^{3/2}}\right\rangle, \quad (4)$$

which depends only on quantities evaluated at the Matsubara poles on the imaginary frequency axis ($i\omega_n$).

To calculate other quantities such as the quasiparticle density of states $N(\nu)$ and the conductivity $\sigma(\nu)$ as a function of the real frequency ν it is necessary to have the gap equations written on the real frequency axis. These equations are more complicated and are[37–39]

$$\begin{aligned}\tilde{\Delta}(\nu+i\delta;\theta)=i\pi T\, g\sum_{m=0}^{\infty}\cos(2\theta)[&\lambda(\nu-i\omega_m)+\lambda(\nu+i\omega_m)]\left\langle \frac{\cos(2\theta')\tilde{\Delta}(i\omega_m;\theta')}{\sqrt{\tilde{\omega}(i\omega_m)^2+\tilde{\Delta}(i\omega_m;\theta')^2}}\right\rangle'\\ &+i\pi\int_{-\infty}^{\infty}dz\,\cos(2\theta)\,I^2F(z)\times[n(z)+f(z-\omega)]\\ &\times\left\langle \frac{\cos(2\theta')\tilde{\Delta}(\nu-z+i\delta;\theta')}{\sqrt{\tilde{\omega}(\nu-z+i\delta)^2-\tilde{\Delta}(\nu-z+i\delta;\theta')^2}}\right\rangle'\end{aligned} \quad (5)$$

and

$$\begin{aligned}\tilde{\omega}(\nu+i\delta)=\nu+i\pi T\sum_{m=0}^{\infty}&[\lambda(\nu-i\omega_m)-\lambda(\nu+i\omega_m)]\times\left\langle \frac{\tilde{\omega}(i\omega_m)}{\sqrt{\tilde{\omega}(i\omega_m)^2+\tilde{\Delta}(i\omega_m;\theta')^2}}\right\rangle'\\ &+i\pi\int_{-\infty}^{\infty}dz\,I^2F(z)[n(z)+f(z-\omega)]\times\left\langle \frac{\tilde{\omega}(\nu-z+i\delta)}{\sqrt{\tilde{\omega}(\nu-z+i\delta)^2-\tilde{\Delta}(\nu-z+i\delta;\theta')^2}}\right\rangle',\end{aligned} \quad (6)$$

with

$$\lambda(\nu)=-\int_{-\infty}^{\infty}d\Omega\ \frac{I^2F(\Omega)}{\nu-\Omega+i0^+}, \tag{7}$$

where now we use the convention that $I^2F(-\Omega)=-I^2F(\Omega)$. The density of quasiparticle states $N(\nu)$ follows from

$$N(\nu)=\left\langle \mathrm{Re}\left\{\frac{\tilde{\omega}(\nu+i0^+)}{\sqrt{\tilde{\omega}(\nu+i0^+)^2-\tilde{\Delta}(\nu+i0^+;\theta)^2}}\right\}\right\rangle, \tag{8}$$

which is normalized to its normal-state value. The conductivity formula[39–48] will be given in Sec. IV after we have presented our numerical results for the penetration depth. We will also make use of Eqs. (5) and (6) in our discussion of the quasiparticle density of states in Sec. III.

III. RESULTS

As described in the work of Williams and Carbotte[36] which is based on the earlier paper of Millis, Sachdev, and Varma,[49] the low-frequency part of the functional derivative of the critical temperature with respect to $I^2F(\Omega)$ is negative at low frequencies for physically meaningful values of g. Following the work of Mitrovic and Carbotte[50] a simplified expression for the functional derivative can be obtained within a two-square-well model for the pairing interaction. We obtain

$$\frac{\delta T_c}{\delta I^2F(\Omega)}\propto G(\overline{\omega}),\quad \overline{\omega}=\frac{\Omega}{T_c}, \tag{9}$$

and

$$G(\overline{\omega})=\sum_{m,m'=-\infty}^{\infty}\frac{1}{|2m-1|}\frac{2\overline{\omega}}{\overline{\omega}^2+4\pi^2(m-m')^2}\left[\frac{g/2}{|2m'-1|}-\frac{\mathrm{sgn}(\omega_m\omega_{m'})}{|2m-1|}\right]. \tag{10}$$

For $m=m'$ in Eq. (10) a term varying like $1/\overline{\omega}$ enters with a nonzero negative coefficient for $g\leqslant 2$. This leads directly to the fact that the exchange of low-frequency bosons described by $I^2F(\Omega)$ reduces the value of the critical temperature. This means that if a low-frequency, temperature-dependent cutoff ω_c is applied to the spectral density $I^2F(\Omega)$, which is maximum at $T=0$ but which gradually goes to zero as the superconducting gap closes up at T_c, the amount of pair breaking present in the system due to inelastic scattering will increase with increasing temperature. This will lead to a value of T_c which is smaller than the value it would have had if the cutoff ω_c had been kept fixed at its zero-temperature value (its maximum value).

A consequence of applying a low-frequency cutoff to $I^2F(\Omega)$ is that T_c initially increases over its value when $\omega_c=0$ as shown in Fig. 1. We show in this figure the value of the ratio of T_c (with cutoff) to its value T_{c0} (without cutoff) and note that the effect can be quite large. For the parameters used in the figure the ratio T_c/T_{c0} has a maximum of about 1.44 near $\omega_c/T_{c0}\simeq 5$, after which T_c starts to decrease again. This decrease is due to the fact that we are now cutting out some bosons in $I^2F(\Omega)$ that contribute positively to the functional derivative. For the computer runs shown in this figure a linearized version of Eqs. (1) and (2) was solved. To be definite we used for the electron-boson spectrum a model which is motivated by the nearly antiferromagnetic Fermi liquid model[25–27] with[49]

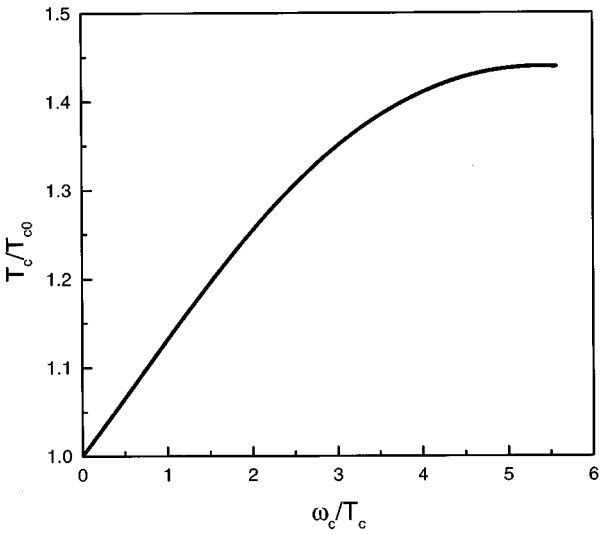

FIG. 1. The value of the normalized critical temperature T_c/T_{c0} with T_{c0} the critical temperature for the case when no low-frequency cutoff is applied to the electron-boson spectral density $I^2F(\Omega)$, as a function of the low-frequency cutoff ω_c/T_{c0}.

$$I^2F(\Omega)=I^2\frac{\Omega/\omega_{\mathrm{sf}}}{1+(\Omega/\omega_{\mathrm{sf}})^2}. \tag{11}$$

In Eq. (11) the strength I^2 is adjusted to ensure a critical temperature $T_{c0}=100$ K; the characteristic boson energy ω_{sf} (= 30 meV) and an upper frequency cutoff $\Omega_{\max}$ (= 400 meV) were chosen to get a strong-coupling parameter of $T_{c0}/\omega_{\log}=0.31$ where $\omega_{\log}$ is defined in the usual way[19] and represents an average boson energy in the system. The only other parameter is g which gives the relative d-to-s admixture in the electron-electron potential. In Fig. 1, $g=0.8$ was chosen as it will be for all the other results to be presented later on. The results of Fig. 1 do not depend qualitatively on our choice of parameters and a different form for $I^2F(\Omega)$ could have been used. In this context Eq. (11) should not be interpreted as a commitment to a spin fluctuation mechanism. It is used mainly to be definite and other forms could have been employed if more definite information about the microscopic mechanism would have been available.

In Figs. 2(a) and 2(b) we show solutions for the real (solid line) and imaginary (dotted line) part of (a) the gap amplitude $\Delta(\nu)$ and (b) the renormalization function $Z(\nu)$ with (lower frame) and without (upper frame) a low-frequency cutoff ω_c. It is clear from Eq. (5) that the pairing energy $\tilde{\Delta}(\nu+i\delta,\theta)$ is anisotropic. However, it is proportional to $\cos(2\theta)$ and can be written as an amplitude $\Delta(\nu)$ times an angular factor, namely,

$$\tilde{\Delta}(\nu+i\delta;\theta)=\tilde{\Delta}(\nu)\sqrt{2}\cos(2\theta). \tag{12}$$

On the other hand, $\tilde{\omega}(\nu+i\delta)$ is isotropic and does not depend on angles. Thus it can be written as $\tilde{\omega}(\nu+i\delta)$

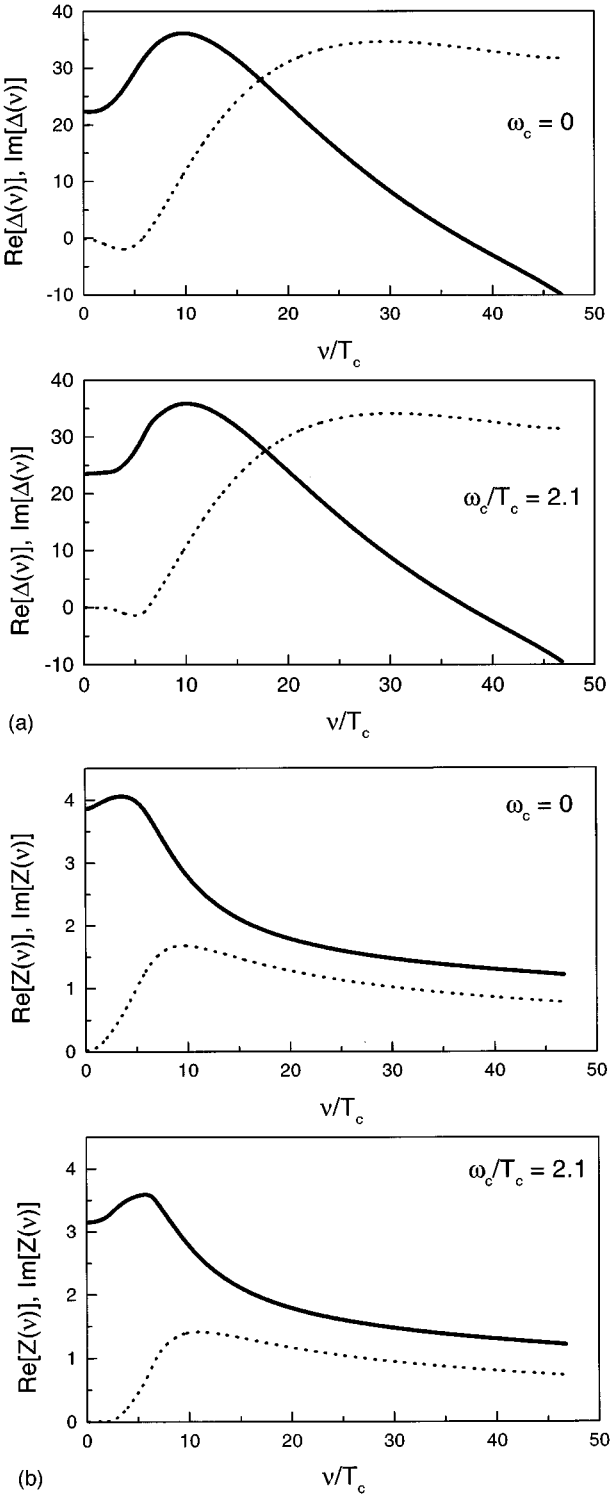

FIG. 2. (a) The top frame shows the real (solid curve) and imaginary (dotted curve) part of the average gap amplitude $\Delta(\nu)$ with $\Delta_{\mathbf{k}}(\nu)\equiv\Delta(\nu)\sqrt{2}\cos(2\theta)$ as a function of the frequency ν/T_c. The parameters are $g=0.8$, reduced temperature $T/T_c=0.1$, and $T_c=100$ K with no low-frequency cutoff (ω_c) applied to the spectral density. The bottom frame is the same as for the top frame except that now a low-frequency cutoff is applied to the electron-boson spectral density with the value $\omega_c/T_c=2.1$. (b) Same as for (a) but now the real and imaginary parts of the renormalization function $Z(\nu)$ are plotted against the normalized frequency ν/T_c. By definition the renormalized Matsubara frequency $\tilde{\omega}(\nu)=\nu Z(\nu)$.

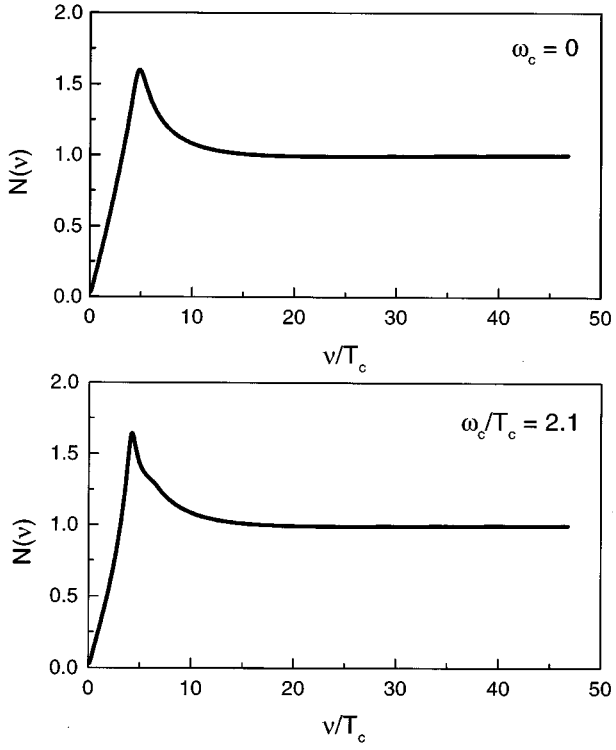

FIG. 3. The quasiparticle density of states $N(\nu)$ based on Eq. (8) vs the normalized frequency ν/T_c. Both frames are for $g=0.8$; the top frame shows results for $\omega_c/T_c=0$, and the bottom frame is for a low-frequency cutoff $\omega_c/T_c=2.1$.

$=\nu Z(\nu)$ where $Z(\nu)$ is the renormalization function. Furthermore, the gap amplitude $\Delta(\nu)$ is related to the pairing energy $\tilde{\Delta}(\nu)$ by $\tilde{\Delta}(\nu)=\Delta(\nu)Z(\nu)$. It is the angular-independent quantities $\Delta(\nu)$ and $Z(\nu)$ that are presented in Fig. 2. A feature to be noted in the lower panels is that the imaginary part of both $\Delta(\nu)$ and $Z(\nu)$ remains essentially zero up to the lower cutoff frequency $\omega_c/T_c=2.1$ in $I^2F(\Omega)$. At higher frequencies the imaginary part of both $\Delta(\nu)$ and $Z(\nu)$ becomes nonzero, initially negative for $\Delta(\nu)$ but always positive for $Z(\nu)$. This is to be contrasted with the results shown in the upper frames in which the imaginary part immediately becomes nonzero for $\nu\neq 0$. This is because no low-frequency cutoff has been applied in this case and the fluctuation spectrum $I^2F(\Omega)$ has a nonzero weight at any finite value of Ω. For reference we note that in Fig. 2 we have used $T_{c0}=100$ K, $T_c/\omega_{\log}=0.31$, $g=0.8$, and a reduced temperature $t=T/T_c=0.1$.

The density of quasiparticle states[49] given by Eq. (8) follows directly from our numerical solutions of Eqs. (5) and (6). Results are given in Fig. 3 for a reduced temperature $t=T/T_c=0.1$. In the top frame no low-frequency cutoff is applied to $I^2F(\Omega)$. An important feature to note about this curve is that the peak in the quasiparticle density of states falls at $\nu/T_c\simeq 4.5$ which corresponds to a large value of Δ/k_BT_c as compared with BCS theory ($=2.2$), and therefore to quite strong coupling (note that $T_c/\omega_{\log}=0.31$). Its magnitude also reflects the low-frequency cutoff ω_c which we have used. Yet no clear boson structure is resolved in the frequency dependence of the density of states. This is due to the fact that the energy scale in $I^2F(\Omega)$ is large (with the

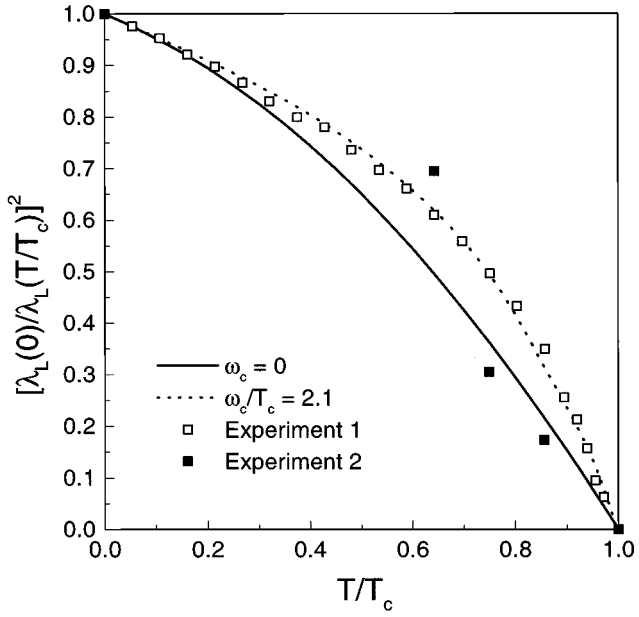

FIG. 4. The inverse square of the normalized London penetration depth $[\lambda_L(0)/\lambda_L(T)]^2$ as a function of the reduced temperature $t=T/T_c$. The solid curve is without a low-frequency cutoff (ω_c) in the electron-boson spectral density while the dotted curve is for $\omega_c/T_c=2.1$. The other parameters are $g=0.8$ and $T_c=100$ K. The open squares represent microwave data (Refs. 29 and 30) and the solid squares are extrapolated from infrared data (Ref. 54).

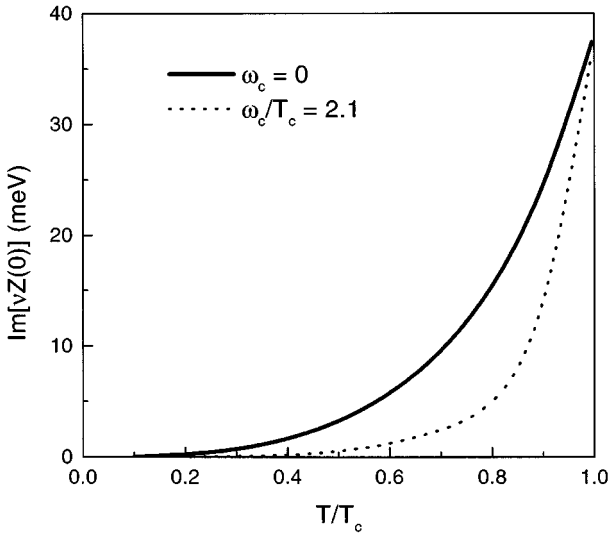

FIG. 5. The imaginary part of renormalization function $\nu Z(\nu\rightarrow 0)$ as a function of the reduced temperature $t=T/T_c$. The solid curve is without the low-frequency cutoff (ω_c) on the electron-boson spectral density while the dotted curve is for $\omega_c/T_c=2.1$. The other parameters are $g=0.8$ and $T_c=100$ K.

high-frequency cutoff at 400 meV) and that it does not have sharp peaks as it would in the case of phonons.[51] Clearly, for an $I^2F(\Omega)$ given by Eq. (11) tunneling spectroscopy will not be as useful in determining the detailed nature of the mechanism involved as it has proved to be in conventional superconductors.[52] The same will hold for any electronic mechanism with a large energy scale even if the coupling is strong.

A distinct structure in the quasiparticle density of states, however, is clearly present in the bottom frame of Fig. 3, giving $N(\nu)$ vs ν/T_c. This structure is directly related to the low-frequency cutoff which is applied to $I^2F(\Omega)$ and it falls at a frequency of $\nu/T_c=\omega_c/T_c=2.1$ above the gap peak in $N(\nu)$. This occurs whatever the value of g. The structure reflects directly the low-frequency cutoff introduced in our model phenomenologically and which is assumed to be due to the onset of superconductivity. While the calculations are not done self-consistently here, they serve to show clearly how a cutoff in the fluctuation spectrum affects $N(\nu)$. Coffey and Coffey[52,53] discussed a similar case within BCS theory. Tunneling spectroscopy should, in principle, allow us to see the gapping of the fluctuation spectrum.

Our results for the temperature dependence of the penetration depth given on evaluation of Eq. (4), which requires only the imaginary frequency version of the gap equations (1) and (2), are displayed in Fig. 4. The solid curve is the result obtained on the basis of the spectrum of Eq. (11) with $T_c=100$ K, $T_c/\omega_{\log}=0.31$, and $g=0.8$ without a low-frequency cutoff. As in previous work[16–18] the slope of the penetration depth near T_c is not sufficiently steep as compared to experiment.[1] If, on the other hand, a low-frequency cutoff equal to $\omega_c/T_c=2.1$ in value at zero temperature is applied, we obtain the dotted curve which is much closer to experimental results shown as open squares. The large difference between these two curves represents the effect of the low-frequency cutoff on $I^2F(\Omega)$ of Eq. (11) which is the largest at $T=0$ K and which is gradually switched off as a function of increasing temperature. In the calculations, the temperature dependence of $\omega_c(T)$ was taken to reflect roughly the temperature variation of the underlying superconducting order parameter. The details are not important. What pushes the curve up at intermediate temperatures and correspondingly increases the slope near $T=T_c$ is the pair-breaking effect associated with the introduction of more low-frequency fluctuations in $I^2F(\Omega)$ as T increases towards T_c. Thus, the difference between the solid and the dotted curve in Fig. 4 is related to the collapse of the quasiparticle scattering time observed in microwave experiments, as a large peak at low temperatures. This was described in the Introduction and will be considered again in detail at the end of this section. It is clear that introducing the cutoff ω_c has greatly improved the agreement with experiment shown by the open squares.[29,30]

The collapse of the scattering rates included in our calculations through a low-frequency cutoff ω_c is also seen clearly in Fig. 5 where we show the imaginary part of the renormalization function $\nu Z(\nu\rightarrow 0)$ as a function of the reduced temperature T/T_c at $\nu\rightarrow 0$. The imaginary part of the renormalized frequency $\tilde{\omega}(0)=\lim_{\nu\rightarrow 0}\nu Z(\nu)$ is directly related to the imaginary part of the self-energy which is a measure of the quasiparticle lifetimes due to the fluctuation spectrum (11). The solid curve applies to the case without a low-frequency cutoff in $I^2F(\Omega)$. It is to be compared with the dotted curve for which the low-frequency cutoff is set at $\omega_c/T_c=2.1$. The other parameters are as before, $T_c=100$ K, $T_c/\omega_{\log}=0.31$, and $g=0.8$. We note that for the solid curve, $I^2F(\Omega)$ has weight all the way down to $\Omega=0$ and the exchange boson will be excited at any temperature, while for the dotted curve the low-lying fluctuations are suppressed at low temperatures

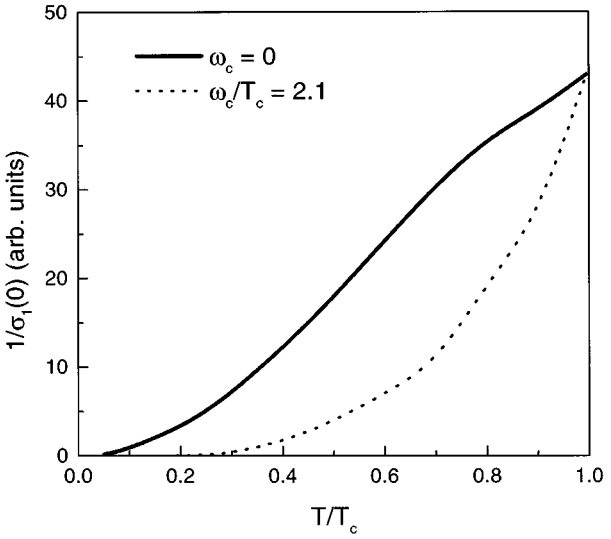

FIG. 6. The zero-frequency value of the inverse of the real part $\sigma_1(\nu=0)$ of the superconducting-state conductivity in arbitrary units as a function of the reduced temperature $t=T/T_c$. The solid curve is without the low-frequency cutoff ($\omega_c/T_c=0$) on the electron-boson spectral density while the dotted curve is for a cutoff of $\omega_c/T_c=2.1$. The other parameters are $g=0.8$ and $T_c=100$ K.

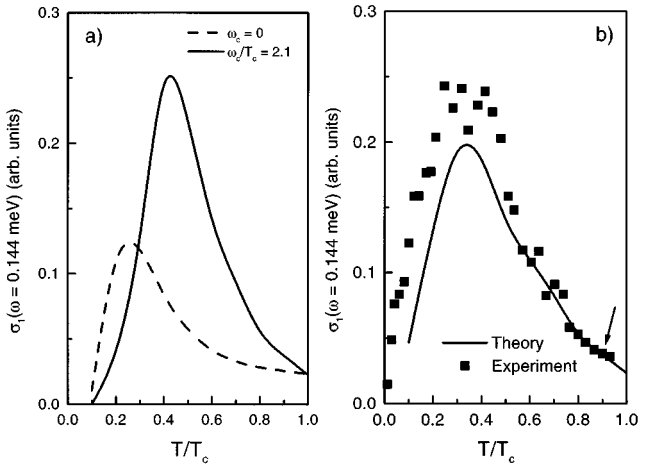

FIG. 7. The microwave conductivity at a frequency of $\nu=0.144$ meV, in arbitrary units, as a function of the reduced temperature $t=T/T_c$. In frame (a) the solid curve is for the case when there is no low-frequency cutoff ($\omega_c/T_c=0$) on the electron-boson spectral density while the dashed curve is for a cutoff of $\omega_c/T_c=2.1$. The other parameters are $g=0.8$ and $T_c=100$ K. Frame (b) includes enough impurity scattering in Born's approximation to reduce the critical temperature from 100 to 95 K. Also shown for comparison are experimental results (solid squares) (Refs. 29 and 30). The arrow indicates the data point which has been used to fit theory to experiment.

and consequently the imaginary part of $\nu Z(\nu\rightarrow 0)$ drops precipitously with decreasing temperature. This precipitous drop is related to the sharp peak observed in the microwave conductivity at low temperatures. This peak enters our work naturally and comes directly from the application of a lower cutoff in $I^2F(\Omega)$. Before giving results for the real part of the microwave conductivity $\sigma_1(\nu)$ as a function of temperature, we show in Fig. 6 its inverse, $1/\sigma_1(\nu)$, for $\nu=0$, i.e., the zero-frequency limit. The results were obtained on the basis of Eq. (16), to be presented in the next section.[39–48] The solid curve is without the low-frequency cutoff in the spectrum (11) while the dashed curve is for $\omega_c/T_c=2.1$. We see that $1/\sigma_1(0)$ behaves very much like the imaginary part of $\tilde{\omega}(\nu=0)$ shown in Fig. 5 and discussed above although the drop with decreasing temperature just below T_c is not as sharp in $1/\sigma_1(\nu=0)$ as in $\tilde{\omega}(\nu=0)$. Nevertheless, the collapse of the quasiparticle scattering rate is reflected in a very rapid reduction of $1/\sigma_1(0)$ as the temperature is reduced below T_c for the cutoff case (dotted line) as compared to the case without cutoff (solid line).

Finally, we show in Fig. 7(a) our results for the temperature dependence of the microwave conductivity $\sigma_1(\nu=0.144$ meV) in arbitrary units. The microwave frequency was chosen to be the higher one of the two values considered in the experiments by Bonn *et al.*[14] The dashed curve is without a cutoff while the solid one is for a low-frequency cutoff $\omega_c/T_c=2.1$. It is clear that, as the value of the lower cutoff is increased, the size of the microwave peak is increased as is the temperature at which it occurs. The results show clearly that the peak in the microwave conductivity which is directly related to the collapse of the quasiparticle scattering rate can be modeled with a low-frequency cutoff in the fluctuation spectrum (11). The application of this cutoff has a large effect on the temperature dependence of the corresponding penetration depth and, in particular, on its slope near T_c. This leads to better agreement with experiment than can be achieved within strong-coupling models that ignore the reaction of the superconducting transition on the fluctuation spectrum itself. This feedback mechanism is clearly effective in changing the shape of the temperature dependence of the penetration depth as it is in the microwave conductivity.

In Fig. 7(b) we compare our results with experimental data (solid squares[1,2]). The solid curve is based on a low-frequency cutoff of $\omega_c/T_c=2.1$ and, in addition, enough static elastic impurity scattering is included so as to reduce T_c by 5° to 95 K. The Born approximation is used to describe the impurity scattering. This has reduced the peak in $\sigma_1(\nu)$ below its value in Fig. 7(a) where no elastic impurity scattering was included and $T_c=100$ K. However, on comparing the solid lines in these two frames it is clear that without impurity scattering the theoretical curve is too narrow and drops towards zero too sharply as the temperature is reduced towards zero. This is not unexpected since the Drude conductivity becomes extremely narrow at low temperatures in a pure case as the inelastic scattering freezes out while impurities will put a lower, temperature-independent limit on its width. It is clear that inclusion of some residual scattering broadens the microwave peak and gives better agreement with experiment (solid squares). On the other hand, the peak height in Fig. 7(b) is a little too low compared with the experimental data. While this is not our aim here, we could get a better fit by increasing the cutoff in the boson spectral density and by changing the amount of elastic scattering employed.

IV. CONDUCTIVITY

The conductivity tensor $\sigma_{jk}(\nu)$ can be written as[39–48]

$$\sigma_{jk}(\nu)=\frac{i}{\nu}\Pi_{jk}(i\nu_n\rightarrow\nu+i0^+), \tag{13}$$

where the analytic continuation from the imaginary boson Matsubara frequencies $i\nu_n$ ($\nu_n=2n\pi T, n=0,\pm1,\pm2,\ldots$) is taken to the real frequency axis $i\nu_n\rightarrow\nu+i0^+$. A standard approximation to $\Pi_{jk}(i\nu_n)$ in which vertex corrections for the electromagnetic interaction are neglected gives

$$\Pi_{jk}(i\nu_n)=\frac{2T}{N}\sum_{m,\mathbf{p}}\mathrm{Tr}\{ev_j(\mathbf{p})G(\mathbf{p},i\nu_n+i\omega_m)\times G(\mathbf{p},i\omega_m)ev_k(\mathbf{p})\}, \tag{14}$$

where v_i is the ith component of the Fermi velocity, $G(\mathbf{p},i\omega_n)$ is the electron Green's function in the 2×2 Nambu matrix notation, and $\mathrm{Tr}\{\cdots\}$ is the trace. In terms of the Matsubara pairing energy $\tilde{\Delta}_{\mathbf{p}}(i\omega_m)$ and the renormalized frequencies $\tilde{\omega}_{\mathbf{p}}(i\omega_m)$ the Green's function has the form

$$G(\mathbf{p},i\omega_m)=\frac{\tilde{\omega}_{\mathbf{p}}(i\omega_m)\tau_0+\epsilon_{\mathbf{p}}\tau_3+\tilde{\Delta}_{\mathbf{p}}(i\omega_m)\tau_1}{\tilde{\omega}_{\mathbf{p}}(i\omega_m)^2-\epsilon_{\mathbf{p}}^2-\tilde{\Delta}_{\mathbf{p}}(i\omega_m)^2}, \tag{15}$$

where τ_0, τ_1, and τ_3 are Pauli matrices and $\epsilon_{\mathbf{p}}$ is the electron dispersion. To get $\Pi_{jk}(i\nu_n)$ on the real frequency axis we need to use the spectral representation for the Green's function. We obtain

$$\Pi_{jk}(\omega+i\delta)=\left\langle 2e^2N(0)v_j(\mathbf{p})v_k(\mathbf{p})\mathrm{Tr}\left\{\int d\epsilon\int d\Omega\ f(\Omega)\frac{-1}{\pi}\mathrm{Im}G(\mathbf{p},\Omega+i\delta)[G(\mathbf{p},\Omega+\omega+i\delta)+G(\mathbf{p},\Omega-\omega-i\delta)]\right\}\right\rangle \tag{16}$$

with

$$G(\mathbf{p},\omega+i\delta)=\frac{\tilde{\omega}_{\mathbf{p}}(\omega+i\delta)\tau_0+\epsilon_{\mathbf{p}}\tau_3+\tilde{\Delta}_{\mathbf{p}}(\omega+i\delta)\tau_1}{\tilde{\omega}_{\mathbf{p}}(\omega+i\delta)^2-\epsilon_{\mathbf{p}}^2-\tilde{\Delta}_{\mathbf{p}}(\omega+i\delta)^2}. \tag{17}$$

After much algebra we arrive at an expression for the conductivity of the form

$$\begin{aligned}\sigma(\nu)=\frac{i}{\nu}\frac{e^2N(0)v_F^2}{2}\Bigg\langle&\int_0^\infty d\Omega\ \tanh\left(\frac{\Omega}{2T}\right)\frac{1}{E(\Omega;\theta)+E(\Omega+\nu;\theta)}[1-N(\Omega;\theta)N(\Omega+\nu;\theta)-P(\Omega;\theta)P(\Omega+\nu;\theta)]\\&+\int_0^\infty d\Omega\ \tanh\left(\frac{\Omega+\nu}{2T}\right)\frac{1}{E(\Omega;\theta)^\star+E(\Omega+\nu;\theta)^\star}[1-N(\Omega;\theta)^\star N(\Omega+\nu;\theta)^\star-P(\Omega;\theta)^\star P(\Omega+\nu;\theta)^\star]\\&+\int_0^\infty d\Omega\left[\tanh\left(\frac{\Omega+\nu}{2T}\right)-\tanh\left(\frac{\Omega}{2T}\right)\right]\frac{1}{E(\Omega+\nu;\theta)-E(\Omega;\theta)^\star}[1+N(\Omega;\theta)^\star N(\Omega+\nu;\theta)+P(\Omega;\theta)^\star P(\Omega+\nu;\theta)]\\&+\int_{-\nu}^0 d\Omega\ \tanh\left(\frac{\Omega+\nu}{2T}\right)\Bigg\{\frac{1}{E(\Omega;\theta)^\star+E(\Omega+\nu;\theta)^\star}[1-N(\Omega;\theta)^\star N(\Omega+\nu;\theta)^\star-P(\Omega;\theta)^\star P(\Omega+\nu;\theta)^\star]\\&+\frac{1}{E(\Omega+\nu;\theta)-E(\Omega;\theta)^\star}[1+N(\Omega;\theta)^\star N(\Omega+\nu;\theta)+P(\Omega;\theta)^\star P(\Omega+\nu;\theta)]\Bigg\}\Bigg\rangle,\end{aligned} \tag{18}$$

with

$$E(\nu;\theta)=\sqrt{\tilde{\omega}_{\mathbf{p}}(\nu+i\delta)^2-\tilde{\Delta}_{\mathbf{p}}(\nu+i\delta)^2}\equiv\sqrt{\tilde{\omega}(\nu+i\delta)^2-\tilde{\Delta}(\nu+i\delta;\theta)^2} \tag{19}$$

and

$$N(\nu;\theta)=\frac{\tilde{\omega}_{\mathbf{p}}(\nu+i\delta)}{E(\nu;\theta)}\equiv\frac{\tilde{\omega}(\nu+i\delta)}{E(\nu;\theta)}, \tag{20}$$

$$P(\nu;\theta)=\frac{\tilde{\Delta}_{\mathbf{p}}(\nu+i\delta)}{E(\nu;\theta)}\equiv\frac{\tilde{\Delta}(\nu+i\delta;\theta)}{E(\nu;\theta)}. \tag{21}$$

The zero-frequency limit of the conductivity, $\sigma_1(\nu=0)$, is calculated by applying L'Hôpital's rule to Eq. (18) to calculate the limit $\nu\rightarrow0$. We find

$$\sigma_1(0)=\frac{e^2N(0)v_F^2}{2}\left\langle \frac{1}{2T}\int_0^\infty \frac{d\Omega}{\cosh^2(\Omega/2T)}\,\frac{1+N_1^2(\Omega,\theta)+N_2^2(\Omega,\theta)+P_1^2(\Omega,\theta)+P_2^2(\Omega,\theta)}{2E_2(\Omega,\theta)}\right.$$

$$-\frac{1}{4T}\int_0^\infty \frac{d\Omega}{\cosh^2(\Omega/2T)}\,\frac{1}{E_1^2(\Omega,\theta)+E_2^2(\Omega,\theta)}\{2E_1(\Omega,\theta)[N_1(\Omega,\theta)N_2(\Omega,\theta)+P_1(\Omega,\theta)P_2(\Omega,\theta)]$$

$$\left.+E_2(\Omega,\theta)[1-N_1^2(\Omega,\theta)+N_2^2(\Omega,\theta)-P_1^2(\Omega,\theta)+P_2^2(\Omega,\theta)]\}\right\rangle, \tag{22}$$

with

$$E(\Omega,\theta)=E_1(\Omega,\theta)+iE_2(\Omega,\theta),$$

$$N(\Omega,\theta)=N_1(\Omega,\theta)+iN_2(\Omega,\theta),$$

$$P(\Omega,\theta)=P_1(\Omega,\theta)+iP_2(\Omega,\theta),$$

according to Eqs. (19)–(21).

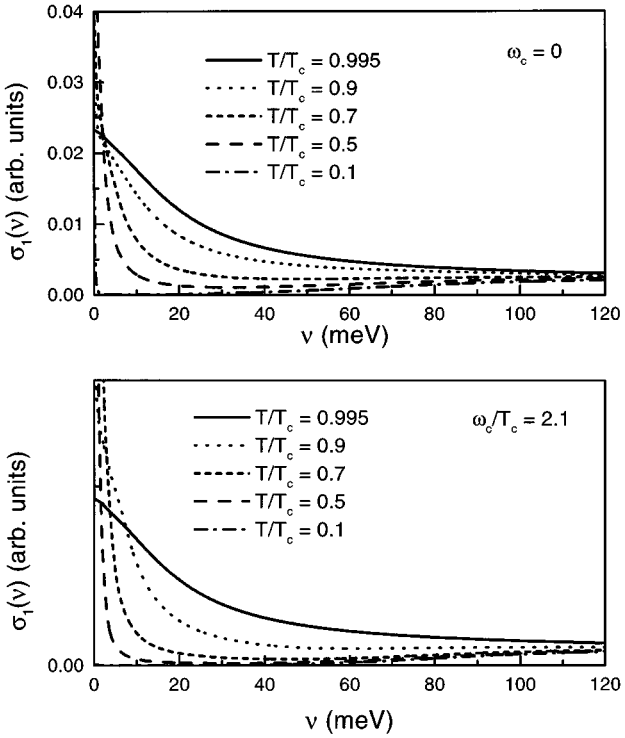

FIG. 8. The real part of the conductivity $\sigma_1(\nu)$ (in arbitrary units) as a function of the frequency ν in meV for five different temperatures $T/T_c=0.995$ (near T_c, solid curve), $T/T_c=0.9$ (dotted curve), $T/T_c=0.7$ (short dashed curve), $T/T_c=0.5$ (dashed curve), and $T/T_c=0.1$ (dash-dotted curve). The bottom frame applies to the case when a low-frequency cutoff of $\omega_c/T_c=2.1$ at zero temperature is applied to the electron-boson spectral density $I^2F(\Omega)$. The top frame is for comparison and does not have a cutoff ($\omega_c/T_c=0$). The application of the low-frequency cutoff leads to a very rapid suppression of the inelastic scattering rate as the temperature is lowered through the critical temperature. The other parameters are $g=0.8$ and $T_c=100$ K.

V. NUMERICAL RESULTS FOR THE CONDUCTIVITY

We present in Fig. 8 our results for the frequency dependence of the real part of the infrared conductivity $\sigma_1(\nu)$ in arbitrary units. The bottom frame includes a low-frequency cutoff of ($\omega_c/T_c=2.1$) in the spectral density $I^2F(\Omega)$ defined in Eq. (11). The top frame is shown for comparison and presents the case without such a cutoff. Five temperature values are considered, namely, one near T_c, at $T/T_c=0.995$ (solid curve), and the others at $T/T_c=0.9$ (dotted curve), $T/T_c=0.7$ (short dashed curve), $T/T_c=0.5$ (dashed curve), and $T/T_c=0.1$ (dash-dotted curve). First we note the narrow Drude peak at low frequencies which sharpens considerably as the temperature is lowered and which is so sharp that it is not seen in the bottom frame on the scale of the graph for the lowest reduced temperature shown, i.e., $T/T_c=0.1$. It is also to be noted that when a low-frequency cutoff is included (bottom frame) the curve at $T/T_c=0.9$ (dotted curve) cuts the solid curve for $T/T_c=0.995$ at a higher frequency than is the case in the upper frame. This is consistent with the fact that with a low-frequency cutoff the inelastic scattering is reduced faster towards zero and the inelastic Drude lifetime goes to infinity more rapidly than without the cutoff. This same trend is seen even more clearly in the short dashed curve for $T/T_c=0.7$. The exact way the Drude-like scattering rate goes to zero depends on the temperature dependence taken for the low-frequency cutoff $\omega_c(T)$ which is assumed to open up very rapidly with decreasing temperature below T_c, reflecting the temperature dependence of the superconducting order parameter. Besides the Drude region described so far, there is a boson-assisted region at higher frequencies which is of less interest here and which, in comparison, is not affected very much by the application of the low-frequency cutoff in $I^2F(\Omega)$.

The differences introduced by the application of a cutoff are more striking for the imaginary part of the conductivity. This is shown in Fig. 9. What is plotted here is the product $\nu\sigma_2(\nu)$ as a function of ν for the same set of five temperatures used in the previous figure, namely, $T/T_c=0.995$ (solid curve), 0.9 (dotted curve), 0.7 (short dashed curve), 0.5 (dashed curve), and 0.1 (dash-dotted curve): As before, the bottom frame applies to a case when a low-frequency cutoff is applied to $I^2F(\Omega)$ while the top frame is without such a cutoff. It is clear that the application of a low-frequency cutoff has a significant effect on both the shapes of the curves and on their absolute magnitudes. At T_c both curves are the same of course, but the solid curves at $T/T_c=0.9$ are already different in the upper and the lower frame. The curves in the bottom frame show a much sharper minimum

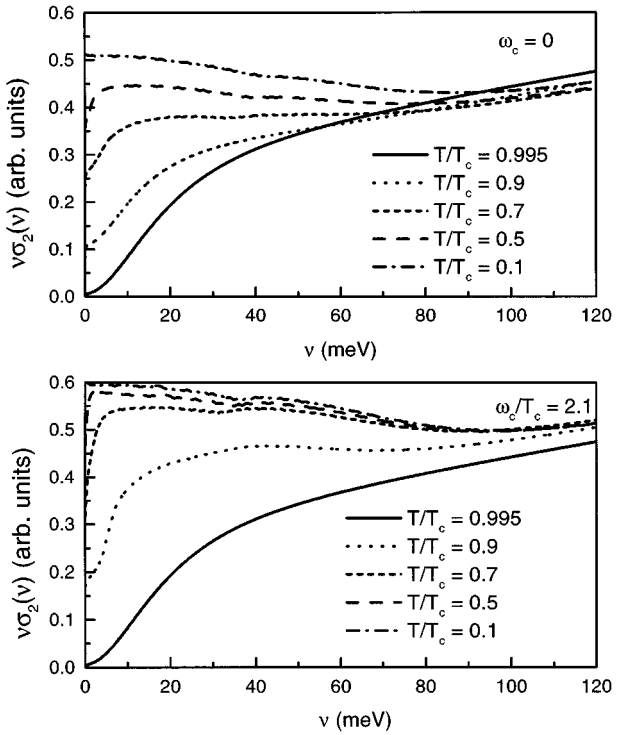

FIG. 9. The imaginary part of the conductivity multiplied by ν, $\nu\sigma_2(\nu)$ (in arbitrary units), as a function of the frequency ν in meV for five different temperatures $T/T_c=0.995$ (very close to T_c, solid curve), $T/T_c=0.9$ (dotted curve), $T/T_c=0.7$ (short dashed curve), $T/T_c=0.5$ (dashed curve), and $T/T_c=0.1$ (dash-dotted curve). The bottom frame applies to the case when a low-frequency cutoff of $\omega_c/T_c=2.1$ at zero temperature is applied to the electron-boson spectral density $I^2F(\Omega)$. The top frame is for comparison and does not have a low-frequency cutoff. The other parameters are $g=0.8$ and $T_c=100$ K.

as a function of frequency around $\nu=0$, reflecting the reduced amount of inelastic scattering in the top frame as compared to the bottom frame. Measurements of the width of these minima in $\nu\sigma_2(\nu)$ at photon energies around $\nu=0$ would allow an inelastic scattering rate to be determined and would show the collapse of the scattering rates which are built into our curves in the bottom frame.

It is clear from these results that, except for the zero-temperature curve which shows no narrow Drude dip at low ν, it is necessary to know $\nu\sigma_2(\nu)$ well in the frequency region below $\nu=5$ meV if we want to extrapolate the data to low ν so as to get the temperature-dependent penetration depth $\lambda(T)$ from formula (4) which involves the limit as $\nu\to 0$. Basov and co-workers[47,48,54] have obtained data on $\nu\sigma_2(\nu)$ in YBCO at several temperatures which show qualitative agreement with our theoretical models.[48] In particular the low-frequency data show no sign of a cusplike structure near twice the superconducting gap value as is expected and seen in an s-wave superconductor.[55] This lack of structure is taken as further evidence for gap nodes crossing the Fermi surface in YBCO. On the other hand, the overall agreement of the finite-temperature data with our results for $\nu\sigma_2(\nu)$ vs ν is not good in a quantitative sense. If the data are extrapolated to get values of the penetration depth $\lambda(T)$ vs T, we obtain the solid squares shown in Fig. 4. It is clear that for $T/T_c\gtrsim 0.7$ the extrapolated infrared results are much too low as compared with the microwave data and our theoretical prediction (dotted curve). Since $\nu\sigma_2(\nu)$ depends on the inverse square of the penetration depth rather than $\lambda^{-1}(T)$ itself, the disagreement between theory and infrared data will be even larger in this case. It is for this reason that the infrared data are not shown in our Fig. 9. Until better agreement can be obtained between infrared and microwave data for the penetration depth it is not possible to conclude whether or not our theoretical approach is correct, or is in need of modifications, or is in serious disagreement with experiment. The potential for such a critical comparison certainly exists and should be pursued.

It has been found useful in the analysis of the frequency dependence of conductivity data to introduce an extended Drude form

$$\sigma(\nu)=\frac{ne^2}{m(\nu)}\left[\frac{1}{\tau^{-1}(\nu)-i\nu}\right], \tag{23}$$

with a frequency-dependent effective mass $m(\nu)$ and a frequency-dependent scattering rate $\tau(\nu)$, both assumed to be real. Equation (23) can be inverted for any frequency-dependent complex function $\sigma(\nu)$ to get

$$\tau^{-1}(\nu)=\frac{\nu\sigma_1(\nu)}{\sigma_2(\nu)} \tag{24}$$

and

$$\frac{m(\nu)}{m}=\frac{ne^2}{m}\frac{\sigma_2(\nu)/\nu}{\sigma_1(\nu)^2+\sigma_2(\nu)^2}. \tag{25}$$

Here we will be particularly interested in the inelastic scattering rate defined by Eq. (24) both as a function of frequency ν and as a function of temperature. In this second instance we are particularly interested in understanding how the collapse of the quasiparticle scattering rate brought about by the application of a low-frequency cutoff in $I^2F(\Omega)$ is reflected in this quantity. The rate $\tau^{-1}(\nu)$ defined in Eq. (24) has the great advantage that it can be extracted directly from experimental data on the conductivity without further analysis.

The scattering rates $\tau^{-1}(\nu)$ which follow from our conductivity curves presented in Figs. 8 and 9 are presented in Fig. 10. Five temperatures, namely, $T/T_c=0.995$ (solid curve), $T/T_c=0.9$ (dotted curve), $T/T_c=0.7$ (short dashed curve), $T/T_c=0.5$ (dashed curve), and $T/T_c=0.1$ (dash-dotted curve), are given. The first feature to be noticed about these curves is the large size of the vertical scale which is given in units of meV. Its value keeps growing with increasing ν in a quasilinear fashion and is roughly of the same magnitude as ν. This very large value of $\tau^{-1}(\nu)$ is in qualitative agreement with experimental data in the oxides[47] and shows that inelastic scattering is very large in these systems as compared with conventional metals. The large amount of inelastic scattering included in our calculations can be traced to the fact that the strong-coupling index associated with the spectrum (11) is large and equal to $T_c/\omega_{\log}=0.31$ which corresponds to the very-strong-coupling regime. This value of $T_c/\omega_{\log}$ is consistent with the fact that the inelastic scattering rate at $T=T_c$ in the oxides is observed to be of the

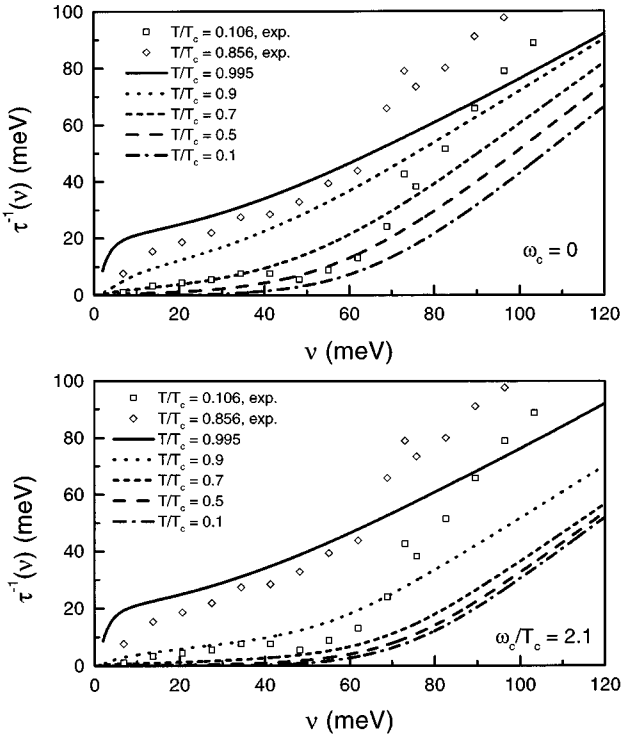

FIG. 10. The frequency dependence of the scattering rate $\tau^{-1}(\nu)$ given by Eq. (24) (in meV) for five different temperatures, namely, $T/T_c=0.995$ (solid curve), $T/T_c=0.9$ (dotted curve), $T/T_c=0.7$ (short dashed curve), $T/T_c=0.5$ (dashed curve), and $T/T_c=0.1$ (dash-dotted curve). The bottom frame applies to the case when a low-frequency cutoff of $\omega_c/T_c=2.1$ at zero temperature is applied to the electron-boson spectral density $I^2F(\Omega)$. The top frame is for comparison and does not have a cutoff. The other parameters are $g=0.8$ and $T_c=100$ K.

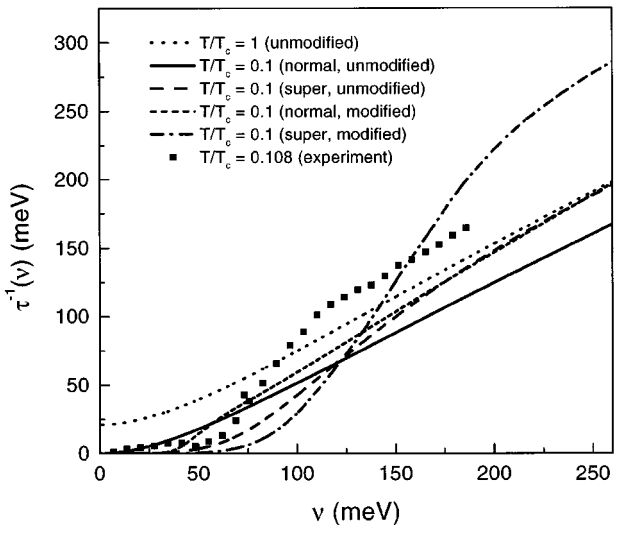

FIG. 11. The conductivity scattering rate $\tau^{-1}(\nu)$ defined in Eq. (24) in meV as a function of ν. Two different models for the spectral density $I^2F(\Omega)$ are used. The first one is the spectrum defined by Eq. (11) and is referred to as unmodified. The second one is obtained from this first one but with a low-frequency cutoff applied up to $\omega_c=30$ meV with spectral weight added between 30 and 40 meV, augmenting $I^2F(\Omega)$ in this region by approximately a factor of 5 (modified spectrum). The solid curve is the normal state at $T/T_c=0.1$ and the dotted is the same but for $T/T_c=1.0$. The long dashed curve is in the superconducting state. These three cases use the unmodified spectrum (11). The other two curves use the modified spectrum and are at $T/T_c=0.1$. The short dashed curve is in the normal state, and the short-dash-dotted one applies to the superconducting state.

same order of magnitude as the value of T_c itself[56] and not fractions thereof, as is the case in conventional superconductors.

The bottom frame of Fig. 10 applies to the case with a low-frequency cutoff in $I^2F(\Omega)$ and is to be compared with the top frame for which there is no cutoff. It is seen that at low ν and $T/T_c=0.9$ the curve for $\tau^{-1}(\nu)$ is much reduced in the bottom frame as compared with the top frame, as we expect. This trend continues as the temperature is reduced further and the lower cutoff is further increased. Shown for comparison on the same graphs are the data[54] at $T/T_c=0.856$ (open diamonds) and $T/T_c=0.106$ (open squares). The high-temperature data agree reasonably well with the dotted curve of the top frame although it is clear that above approximately 60 meV the experimental scattering rate is considerably larger than we calculate. This is also true for the low-temperature data and may indicate that for the higher frequencies shown, there may be an interband transition contribution in the data which has not been included in the theory. Interband transitions have recently been discussed in the work of Atkinson and Carbotte.[57] At low ν there also appear to be some scattering processes in the data that are not included in our theory.

The effect of a d-wave superconducting transition on the transport scattering rate $\tau^{-1}(\nu)$ vs ν and of the details of the fluctuation spectrum $I^2F(\Omega)$ can be understood better with the help of Fig. 11. In this figure we present results for $\tau^{-1}(\nu)$ vs ν in two model cases. Three curves are for the normal state and two for the superconducting state. Three of the curves apply to the case of $I^2F(\Omega)$ given in Eq. (11) without modification. Two involve a modified spectrum with a low-frequency cutoff applied at $\omega_c=30$ meV and an additional spectral weight added in the region $30\leqslant\Omega\leqslant40$ meV of an amount equal to roughly 5 times its value in Eq. (11) for $\Omega=30$ meV. The solid and dotted curves are for the normal state based on spectrum (11) at $T/T_c=0.1$ (low temperature) and $T/T_c=1.0$. On comparison of these two curves we note first of all that the solid curve goes to zero as $\nu\rightarrow0$ while the dotted curve has a finite intercept with the horizontal axis. At any finite temperature scattering of the charge carriers off real, thermally excited bosons leads to a Drude-like conductivity with temperature-dependent scattering times replacing the constant residual scattering present in the case of elastic impurity scattering. This gives a finite intercept in Fig. 11 at low ν. This intercept is very temperature dependent and vanishes at $T=0$. Except for a nearly constant shift upward of the dotted curve it is almost, but not precisely, parallel to the solid ($T\approx0$) curve. The bosons have a second effect on the conductivity curves. Even at zero temperature they lead to boson-assisted absorption in which part of the photon energy goes into the excitation of a boson with overall energy and momentum conservation. These processes are nearly temperature independent and have an onset in the normal state at the lowest boson

energy available in the fluctuation spectrum $I^2F(\Omega)$. For the unmodified spectrum (11) this is zero frequency. Thus absorption and consequently the scattering rate $\tau^{-1}(\nu)$ at zero temperature (solid curve) will begin to rise from zero at $\nu=0$. The sharpness of this rise will depend on the boson density available. We note in particular that for the case when the spectral density $I^2F(\Omega)$ rises like Ω at low values of Ω the charge-carrier–quasiparticle scattering rate will increase as ν^2. These considerations apply only at low ν. At higher ν our calculated scattering rates are found to be quasilinear in agreement with experiment,[47] and large — of the order of the frequencies themselves. Comparison of solid and dotted curves shows that the boson-assisted processes at $T=10$ and 100 K are very similar. As previously mentioned the two curves are nearly parallel.

The dashed curve in Fig. 11 is also in the normal state and for low temperatures. It is now based on the modified spectrum. It is clear now that $\tau^{-1}(\nu)$ is identically zero up to ω_c and then rises somewhat more sharply with ν beyond ω_c than does the solid curve centered about zero. This is expected because the modified $I^2F(\Omega)$ used in the dashed curve has a discontinuous rise at ω_c. Also beyond roughly $\nu\simeq 60$ meV the dashed curve falls above the solid one because of the additional weight in the modified model for $30\leqslant\Omega\leqslant 40$ meV. This added weight is also the reason why the dashed and solid curves do not meet even at $\nu=250$ meV where the dashed line is nearly as large as the dotted curve (which is for $T=100$ K).

For the superconducting state two sets of results are presented. Both are for $T/T_c=0.1$, i.e., low temperatures. The long dashed curve uses the unmodified spectrum (11) and is to be compared with the solid curve in the normal state with the same spectrum. On comparison of the two curves it is seen that superconductivity simply depresses in a smooth way $\tau^{-1}(\nu)$ at small ν in the gap region and enhances it at larger values of ν. These are the characteristics of the superconducting transition to a d-wave symmetry as the same fluctuation spectrum has been used in both cases. It becomes clear, however, that there is no characteristic sharp structure in $\tau^{-1}(\nu)$ vs ν corresponding to twice the superconducting gap value as would be the case for an s-wave superconductor. In such a case $\sigma_1(\nu)$ would be entirely zero in this energy range as would be the scattering rate according to Eq. (24). It is this region that contains the information on the gap symmetry. The high-ν region is more directly related to mechanism. It is not surprising that there is no sharp structure in $\tau^{-1}(\nu)$ corresponding to a gap in the d-wave case and that it looks very much like the normal state but with an additional reduction in the scattering rate at low ν. This is because a condensate forms and removes electrons from the normal fluid but the quasiparticle density of states remains finite (linear in ν) at any finite ν. The final dash-dotted curve in Fig. 11 is again in the superconducting state at a low temperature ($T/T_c=0.1$) but now the modified spectrum is used. In comparing with the dashed curve for the normal state with the same spectrum we see the characteristic reduction at low ν (between 30 and approximately 120 meV) with an overshoot beyond that energy range. Comparing with the long dashed curve, also for the superconducting state but with the unmodified spectrum (11), shows that the details of $I^2F(\Omega)$ do affect the quantitative behavior of the curves but there is no easily identifiable sharp qualitative change. Similar remarks hold when one compares the normal and superconducting states for the d-wave case. The experimental data given in Ref. 47 for $\tau^{-1}(\nu)$ vs ν are shown as the solid squares in Fig. 11 and are for the superconducting state at low temperature. On comparing with the dash-dotted curve it is clear that the agreement is not good although it could be improved by lowering the value of the low-frequency cutoff so that the scattering rate starts its main rise at lower energies. Also we would need to take the spectral weight out at higher energies so as to moderate the overshoot of $\tau^{-1}(\nu)$ at high ν. The value of carrying out such a procedure to produce a better fit is not clear as we now discuss.

Our choice of the model spectrum with a low-frequency cutoff at 30 meV and added weight between 30 and 40 meV was partially motivated by the observation of the so-called ''41 meV peak'' in neutron scattering measurements of the spin susceptibility in YBCO at optimum doping.[58,59] It should be pointed out that this peak and the redistribution of the spectral weight observed on entrance to superconductivity and the comparison with the normal case above T_c are limited to the (π,π) point in the two-dimensional CuO_2 Brillouin zone, i.e., at the antiferromagnetic wave vector. By contrast it is the spin susceptibility everywhere in the first Brillouin zone that determines the spectral function $I^2F(\Omega)$ of Eq. (11) although the (π,π) transitions are expected to be the most important ones in the nearly antiferromagnetic Fermi liquid model. Because of these complications, it is not possible to make a straightforward quantitative comparison between neutron data and optical data at this point. The details of this relationship are yet to be worked out. Nevertheless, it is quite clear from the results presented in Fig. 11 that optical data in the form of $\tau^{-1}(\nu)$ defined by Eq. (24) can be used to obtain information about the mechanism and about the readjustments in the charge-carrier–boson spectral density involved that might be brought about by superconductivity and reductions in temperature. These conclusions are model independent although based on the assumption that Fermi liquid theory can be applied and that some kind of boson-exchange mechanism is responsible for superconductivity. It should be remembered, however, that there could be a significant interband contribution in the data which would need to be understood[57] before definite conclusions can be drawn.

VI. CONCLUSION

The observed large peak in the temperature dependence of the microwave conductivity $\sigma_1(\nu)$ observed in YBCO (Ref. 1) has been interpreted in terms of the collapse of the quasiparticle scattering rates due to the gapping of the fluctuation spectrum responsible for the pairing interaction. We have modeled this gapping in terms of a low-frequency cutoff on the electron-boson spectral density appearing in generalized Eliashberg equations with a separable d-wave model in the gap channel. This allows the discussion of inelastic effects and is the simplest first step beyond BCS theory. The application of a low-frequency cutoff in the fluctuation spectrum of the order needed to model the observed peak in the microwave conductivity leads to large effects in the temperature variation of the resulting magnetic penetration depth.

This brings the curve closer to experiment than is the case when such a cutoff is not applied. While our calculations are admittedly based on a phenomenological model they do show clearly how the collapse of the scattering times is seen in the microwave data and the magnetic penetration depth. We find also that these effects can be large and lead to a novel interpretation of the penetration depth data.

We have also investigated how the application of a low-frequency cutoff in the spectral density $I^2F(\Omega)$ affects the frequency dependence of the infrared conductivity. The Drude peak in the real part of the conductivity at low frequencies sharpens up more rapidly with decreasing temperature than would be the case if no cutoff was present. Also, the product of ν times the imaginary part of σ, $\nu\sigma_2(\nu)$, shows sharper structures in the form of a low-frequency minimum around $\nu=0$ and is also changed considerably in magnitude. Because of the sharp variation in $\nu\sigma_2(\nu)$ at low ν, accurate infrared data in the region below $\lesssim 5$ meV are needed to derive from such information the penetration depth. The collapse of the inelastic scattering rate can also be seen, in principle, in the ν dependence of the scattering rate $\tau^{-1}(\nu)$, Eq. (24). The low-frequency part of such curves reflects not only the symmetry of the order parameter in the superconducting state but also the onset of inelastic scattering. Because the superconducting order parameter is *d* wave, $\sigma_1(\nu)$ is depressed over its normal-state value but is still finite at any frequency below twice the maximum gap and so $\tau^{-1}(\nu)$ is not zero in this region as would be the case for an *s*-wave gap. While it is this range of frequencies that carries most directly the information about the symmetry of the order parameter, the shape of the excitation spectrum, i.e., the spectral density, also affects this region. This can be realized by noting that in the normal state at zero temperature there would be no absorption until the minimum boson energy in $I^2F(\Omega)$ (ω_c) and so $\tau^{-1}(\nu)$ would be zero and starts rising only above ω_c. At higher frequencies the scattering rate reflects directly the amount of inelastic scattering present and, in that sense, this region reflects the mechanism. In our model it has a quasilinear rise, reflecting a general property of a spin fluctuation mechanism which is reasonably flat over a large energy range. The quasilinear frequency dependence seen in our model is in general agreement with the experimental data although our calculations underestimate the amount of inelastic scattering present. In interpreting the data it may be necessary to include interband transitions[57] which make an additional contribution to the scattering rate and which have not been included in this work. Nevertheless, it is clear from our present work that the frequency dependence of the scattering rate carries information about some of the details of the fluctuation spectrum involved and its readjustment with the superconducting transition. For example, should the spectral density be strongly dominated by the imaginary part of the spin susceptibility at (π,π), the so-called 41 meV peak seen to appear in the superconducting state in neutron scattering experiments should have a strong effect on the frequency dependence of the scattering rate. At present comparison with experiment is inconclusive on this part but the opportunity to study with optical techniques the magnetic spin susceptibility or the spectral density of the operative mechanism, should it not be the magnetic fluctuations, remains. While there remain problems with frequency dependence, the temperature dependence of the scattering rate is modeled satisfactorily in our work.

ACKNOWLEDGMENTS

Research was supported in part by the Natural Sciences and Engineering Research Council of Canada (NSERC) and by the Canadian Institute for Advanced Research (CIAR). We thank D. Basov and T. Timusk for access to their data and for discussions.

[1] W. N. Hardy *et al.*, Phys. Rev. Lett. **70**, 3999 (1993).
[2] D. A. Bonn *et al.*, Phys. Rev. B **50**, 4051 (1994).
[3] B. O. Wells *et al.*, Phys. Rev. B **46**, 11 839 (1992).
[4] Z. X. Shen *et al.*, Phys. Rev. Lett. **70**, 1553 (1993).
[5] J. F. Annett and X. Goldenfeld, J. Low Temp. Phys. **89**, 197 (1992).
[6] H. Ding *et al.*, Phys. Rev. B **50**, 1333 (1994).
[7] H. Ding *et al.*, Phys. Rev. Lett. **74**, 2784 (1995); **75**, 1425(E) (1995).
[8] J. Ma, C. Quitmann, R. J. Kelley, H. Beyer, G. Margaritondo, and M. Onellion, Science **267**, 862 (1995).
[9] D. A. Wollmann *et al.*, Phys. Rev. Lett. **71**, 2134 (1993).
[10] D. A. Brawner and H. R. Ott, Phys. Rev. B **50**, 6530 (1994).
[11] P. Chaudhari and S. Y. Lin, Phys. Rev. Lett. **72**, 1084 (1994).
[12] A. G. Sun *et al.*, Phys. Rev. Lett. **72**, 2267 (1994).
[13] C. C. Tsuei *et al.*, Phys. Rev. Lett. **73**, 593 (1994).
[14] D. A. Bonn, D. C. Morgan, K. Zhang, R. Liang, D. J. Baar, and W. Hardy, J. Phys. Chem. Solids **54**, 1297 (1993).
[15] M. Prohammer and J. P. Carbotte, Phys. Rev. B **43**, 5370 (1991).
[16] P. Arberg, M. Mansor, and J. P. Carbotte, Solid State Commun. **86**, 671 (1993).
[17] P. Arberg, M. Mansor, and J. P. Carbotte, J. Phys. Chem. Solids **54**, 1461 (1993).
[18] J. P. Carbotte and C. Jiang, Phys. Rev. B **48**, 4231 (1993).
[19] J. P. Carbotte, Rev. Mod. Phys. **62**, 1027 (1990).
[20] N. Bulut and D. J. Scalapino, Phys. Rev. B **50**, 16 078 (1994).
[21] D. J. Scalapino, J. Phys. Chem. Solids **54**, 1433 (1993).
[22] S. Kamal, D. A. Bonn, N. Goldenfeld, P. J. Hirschfeld, R. Liang, and W. N. Hardy, Phys. Rev. Lett. **73**, 1845 (1994).
[23] D. J. Scalapino, E. Loh, and J. E. Hirsch, Phys. Rev. B **34**, 8190 (1986).
[24] N. E. Bickers, R. T. Scalettar, and D. J. Scalapino, Int. J. Mod. Phys. B **1**, 687 (1987).
[25] A. J. Millis, H. Monien, and D. Pines, Phys. Rev. B **42**, 167 (1990).
[26] P. Monthoux, A. V. Balatsky, and D. Pines, Phys. Rev. Lett. **67**, 3448 (1991).
[27] P. Monthoux and D. Pines, Phys. Rev. B **47**, 6069 (1993).
[28] M. C. Nuss, P. M. Mankiewich, M. L. O'Malley, E. H. Westerwick, and P. B. Littlewood, Phys. Rev. Lett. **66**, 3305 (1991).
[29] D. A. Bonn, P. Dosanjh, R. Liang, and W. H. Hardy, Phys. Rev. Lett. **68**, 2390 (1992).
[30] D. A. Bonn, R. Liang, T. M. Risemann, D. J. Baar, D. C. Morgan, K. Zhang, P. Dosanjh, T. L. Duty, A. MacFarlane, G. D. Morris, J. H. Brewer, W. N. Hardy, C. Kallin, and A. J. Berlinsky, Phys. Rev. B **47**, 11 314 (1993).

[31] C. M. Varma, Int. J. Mod. Phys. B **3**, 2083 (1989).
[32] Y. Kuroda and C. M. Varma, Phys. Rev. B **42**, 8619 (1990).
[33] E. J. Nicol and J. P. Carbotte, Phys. Rev. B **44**, 7741 (1991).
[34] J. P. Carbotte and E. J. Nicol, Physica C **185-189**, 162 (1991).
[35] J. M. Daams and J. P. Carbotte, Solid State Commun. **34**, 599 (1980).
[36] P. J. Williams and J. P. Carbotte, Phys. Rev. B **39**, 2180 (1989).
[37] J. P. Carbotte and C. Jiang, Phys. Rev. B **49**, 6126 (1994).
[38] F. Marsiglio, M. Schossmann, and J. P. Carbotte, Phys. Rev. B **37**, 4965 (1988).
[39] R. Akis, J. P. Carbotte, and T. Timusk, Phys. Rev. B **43**, 12 804 (1991).
[40] W. Lee, D. Rainer, and W. Zimmermann, Physica C **159**, 535 (1989).
[41] N. E. Bickers, D. J. Scalapino, R. T. Collins, and Z. Schlesinger, Phys. Rev. B **42**, 67 (1990).
[42] E. J. Nicol, J. P. Carbotte, and T. Timusk, Phys. Rev. B **43**, 473 (1991).
[43] F. Marsiglio, R. Akis, and J. P. Carbotte, Phys. Rev. B **45**, 9865 (1992). This reference provides a derivation of the phonon self-energy at $q=0$ which is almost identical to the conductivity.
[44] S. B. Nam, Phys. Rev. **156**, 470 (1967); **156**, 487 (1967).
[45] O. V. Dolgov, E. G. Maksimov, and S. V. Shluga, in *Electron-Phonon Interaction on Oxide Superconductors*, edited by R. Baquero (World Scientific, Singapore, 1991), p. 30.
[46] C. Jiang and J. P. Carbotte, J. Supercond. **7**, 559 (1994).
[47] J. P. Carbotte, C. Jiang, D. Basov, and T. Timusk, Phys. Rev. B **51**, 11 798 (1995).
[48] C. Jiang, E. Schachinger, J. P. Carbotte, D. Basov, and T. Timusk, Phys. Rev. B **54**, 1264 (1996).
[49] A. J. Millis, S. Sachdev, and C. M. Varma, Phys. Rev. B **37**, 4975 (1988).
[50] B. Mitrovic and J. P. Carbotte, Solid State Commun. **37**, 1009 (1981).
[51] W. L. McMillan and J. Rowell, in *Superconductivity*, edited by R. D. Parks (Dekker, New York, 1969), p. 561.
[52] D. Coffey, J. Phys. Chem. Solids **54**, 1369 (1993).
[53] D. Coffey and L. Coffey, Phys. Rev. Lett. **70**, 1529 (1993).
[54] D. Basov (private communication).
[55] F. Marsiglio, J. P. Carbotte, A. Puchkov, and T. Timusk, Phys. Rev. B **53**, 9433 (1996).
[56] Y. Zha, S. L. Cooper, and D. Pines, Phys. Rev. B **53**, 8253 (1996).
[57] W. A. Atkinson and J. P. Carbotte, Phys. Rev. B **55**, 3230 (1997).
[58] P. Bourges, L. P. Regnault, Y. Sidis, and C. Vettier, Phys. Rev. B **53**, 876 (1996).
[59] H. F. Fong, B. Keimer, P. W. Anderson, D. Reznik, F. Dogan, and I. A. Aksay, Phys. Rev. Lett. **75**, 316 (1995).